Crack Profiles in Mortar Measured by Holographic Interferometry

by R.A. Miller, S.P. Shah and H.I. Bjelkhagen

ABSTRACT—In order to test the accuracy of theoretical fracture models for mortar and concrete, it is necessary to have accurate measurements of the crack profiles. In this study, sandwich holographic interferometry has been used to find the crack profiles in a center-notched plate specimen loaded at the center of the notch. The results have shown that at low load levels with corresponding short crack lengths, there is little difference between the measured crack profiles and elastic crack profiles computed by finite-element analysis. At high loads with long crack lengths there is a large difference between measured and computed elastic crack profiles. The data suggest the presence of a closing pressure at the crack tip and that there may be a limit to crack-tip-opening displacement (CTOD) before the crack propagates.

Introduction

It is generally accepted that nonlinear fracture models must be used to describe the cracking process in mortar. Several authors[5,7,9,12,15] have proposed models in which a closing pressure is applied to the crack. One way to test which of these models is appropriate is to compare the model predictions with measured crack-opening profiles. Most researchers measure the crack-opening displacement (COD) at one or two discrete points and make their comparisons with these few measurements. Until now, no one has been able to accurately measure the entire crack-opening profile in concrete or mortar.

Laser holographic interferometry is ideally suited to measuring surface-crack-opening profiles. This method allows surface displacements to be measured across the entire object with an accuracy of less than 1 μm. Cracks are easily seen as discontinuities in the fringe pattern formed by the interferometry process. This allows cracks to be seen anywhere on the surface long before they are visible to the eye.

Previous attempts have been made to study cracking in concrete using laser holographic interferometry and an excellent summary of these efforts can be found in Jacquot and Rastogi.[8] Most of these previous studies used holographic interferometry to observe crack patterns and to measure out of plane (perpendicular to the object surface) displacement. To the best of the authors' knowledge, no one has used holographic interferometry to obtain crack-opening displacements in mode I cracks in concrete or mortar.

Holographic Interferometry

A hologram is a complex diffraction grating which, when illuminated by a properly oriented beam of laser light, reproduces a three-dimensional image of an object. The hologram is formed by recording the interference pattern of two light waves, the object wave and the reference wave. Object waves are formed by reflecting an expanded beam of laser light off an object onto a photographic material, while the reference wave is an expanded, but otherwise undisturbed, beam of laser light that is shone directly onto the photographic material. The two waves interfere and the interference pattern is recorded in the photographic emulsion. If the photographic material is developed, replaced in its original position, and then illuminated by the reference wave, the reference wave will be diffracted by the recorded interference patterns and reproduce an exact duplicate of the original object wave.

Since the reproduced object wave is made of laser light, it is possible to interfere with this wave. In holographic interferometry, two object waves, representing the object in two different states of deformation, are combined. The two waves then interfere with each other resulting in an image of the object covered with alternate light and dark fringes. These fringes quantitatively represent the movement, which occurred between the making of the two holograms, of each point on the object surface.

The type of interferogram used in this study is called a sandwich hologram. Sandwich holograms are made by taking two separate holograms of the object in two different states of displacement and, after processing, gluing the holograms together. (The actual process is more complicated than this and has been omitted in the interest of brevity. Information on making sandwich holograms can be found in Abramson.[1]) One of the problems with most types of interferograms is that they will record the effects of all displacements, including rigid-body displacements. Fringe patterns created by rigid-body motion can obscure

R.A. Miller (SEM Member) is Graduate Research Assistant, Department of Civil Engineering; S.P. Shah (SEM Member) is Professor of Civil Engineering and Director of the Center for Concrete and Geomaterials; and H.I. Bjelkhagen is Associate Professor of Biomedical Engineering, Northwestern University, Evanston, IL 60208.

Original manuscript submitted: September 25, 1987. Final manuscript received: May 20, 1988.

the fringe patterns created by stress-induced displacements, rendering the interferogram useless. The advantage to sandwich holography is that the effects of rigid-body motion can be eliminated by rotating the sandwich hologram about a particular axis.[1,2]

Specimen

The specimen used in this study was a center-cracked plate loaded by point loads at the midpoint of the crack (Fig. 1). This specimen was similar to the one used by Kesler, Naus, and Lott.[11] Originally Kesler *et al.* concluded from the data collected from these specimens that linear-elastic fracture mechanics (LEFM) could not be used for concrete or mortar.

Saouma, Ingraffea, and Catalano[14] later reanalyzed the data of Kesler *et al.*[14] using a finite-element program and concluded that Kesler *et al.* had used an incorrect expression for K_{IC} (mode I critical-stress-intensity factor) and had not accounted for stable crack growth. By using a finite-element program to calculate K_{IC} and accounting for stable crack growth resulting from the finite dimensions of the specimen, Saouma *et al.* concluded that LEFM was applicable.

The conclusions of Saouma *et al.*[14] were disputed by Bazant and Oh[5] who showed that both linear and nonlinear theories would give similar results as far as loads were concerned. However, they argued that strains in front of the crack measured by Kesler *et al.*[11] supported nonlinear theories.

The actual specimen used in this study was a mortar plate 12 × 12 × 1 in. (305 × 305 × 25 mm). A 1-in. (25-mm) loading hole with two diametrically opposed notches was cast into the center of the plate. The length of the notches, measured from the center of the loading hole, was 7/8 in. (22 mm). The mortar used to cast the specimens had ratios of 1.00/2.60/0.65 (cement/sand/water) by weight. The compressive strength of each batch of mortar was determined by testing 3-in. × 6-in. (76-mm × 152-mm) cylinders just after specimens made from that batch were tested (Table 1). The elastic modulus was calculated using the equation given in the *Building Code Requirements for Reinforced Concrete* (ACI-318-83):[3]

$$E_c = \zeta w^{1.5} \sqrt{f_c'} \qquad (1)$$

where E_c = elastic modulus (in psi, MPa); $\zeta = 33$ if E_c in psi and w in pfc, and $\zeta = 0.043$ if E_c in MPa and w in kg/m³; w = unit weight (130 pfc, 2100 kg/m³); f_c' = compressive strength (in psi, MPa).

After casting, the specimens were cured in tanks filled with lime water until needed, usually about 90 days. The specimens were removed from the tanks two days before testing and allowed to dry. Before testing, the specimens were coated with Magnaflux developer (SKD-NF/ZP-9B) to provide a diffuse reflective surface for making holograms. The developer is similar to a talcum powder and no surface film is formed.

TABLE 1—COMPRESSIVE STRENGTH OF MORTAR PLATE SPECIMENS

Date of Test	f_c' psi	f_c' MPa	E_c psi	E_c MPa
1/8/87	4150	29	3.2×10^6	22100
1/30/87	6890	47.5	4.1×10^6	28300
1/31/87	6890	47.5	4.1×10^6	28300
2/15/87	6810	47	4.0×10^6	27600

A total of four specimens were tested. The specimens were tested in 20,000-lb (90-kN) capacity loading frame mounted on a vibration isolation table. Loading was accomplished by using the 'airplane' shaped pieces shown in Figs. 1(b) and (2). The 'nose' of the 'airplane' is attached to a semicylindrical piece which applies the load to the specimen loading hole. Strain-gaged steel bars connect the 'wings' and, since they are loaded in parallel with the concrete, stabilize the growth of the crack in the concrete. The load in the concrete is determined by subtracting the load in the steel, as measured by the strain gages, from the total load read from a load cell.

Holographic Arrangement

The holograms used in this experiment were split-beam transmission (Leith-Upatnieks type) holograms, as shown in Fig. 1 [note the black box next to the plate holder in

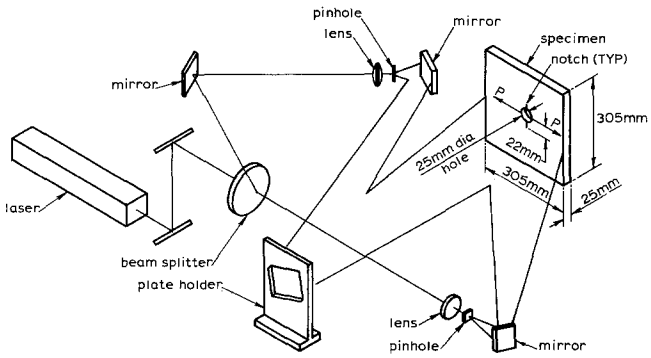

(a)

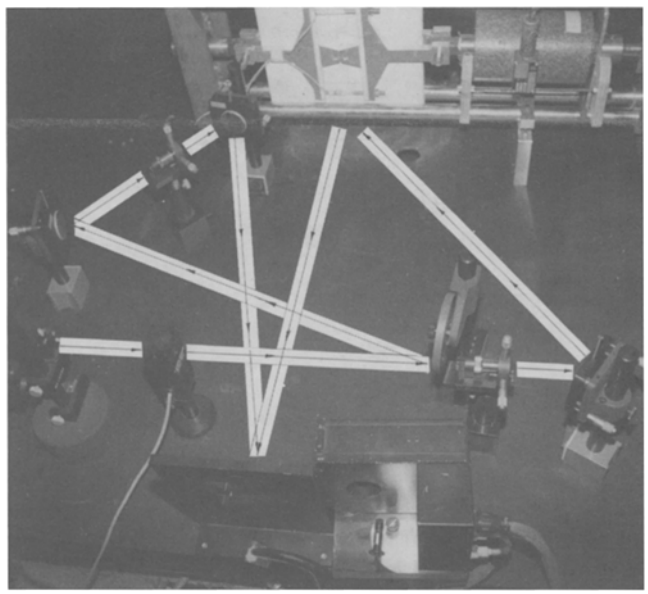

(b)

Fig. 1—(a) Holographic arrangement and (b) specimen dimensions

Fig. 1(b) is a monobath holographic film processor used to check the holographic system]. A laser beam is split into two parts, one part illuminates the object and creates the object wave, while the other part of the beam creates the reference wave. A HeNe laser ($\lambda = 2.5 \times 10^{-5}$ in., 633 nm) was used.

One important parameter in the holographic arrangement is the sensitivity vector, $\vec{k}$. The sensitivity vector is the bisector of the angle formed by the beam illuminating the object and the beam reflected from the object to the photographic plate (Fig. 3). The fringe pattern seen in a holographic interferogram can be thought of as representing the projection of the surface displacement on the sensitivity vector. The displacement, $\vec{d}$, is found to be[1]

$$\vec{d} \cdot \vec{k} = \frac{n\lambda}{2 \cos \alpha} \qquad (2a)$$

or, solving the dot product,

$$d = \frac{n\lambda}{2 \cos \alpha \cos \delta}$$

where n = fringe order, λ = wavelength of laser light, $\alpha = \frac{1}{2}$ angle between beam illuminating the object and beam reflected from object to the photographic plate, and δ = angle between $\vec{d}$ and $\vec{k}$.

In these experiments, three different orientations of the sensitivity vector were used. Holograms are not sensitive to motions perpendicular to the sensitivity vector,[1] so to measure in-plane motion (x direction, see Fig. 2 for axes) the sensitivity must have an in-plane component. Two specimens were tested with the sensitivity vector at 63 deg from the surface and one specimen was tested with the sensitivity vector at 70 deg to the surface. It was possible to measure in-plane motions for these three specimens. The last specimen had a sensitivity vector at 90 deg to the surface and was sensitive only to out of plane (z direction) motions (Table 2).

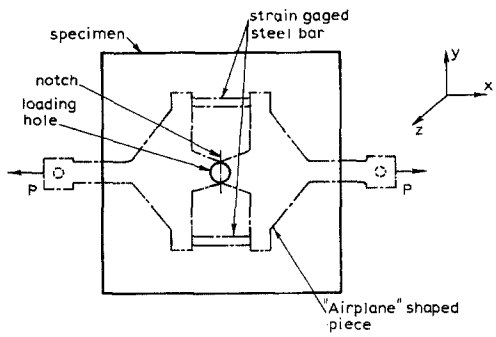

Fig. 2—Loading device

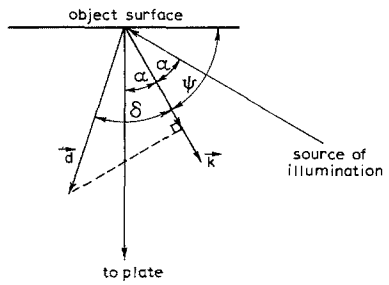

Fig. 3—Definition of the sensitivity vector, $\vec{k}$

Because holograms are sensitive to vibration, all experiments were conducted on a vibration-isolation table. The table was placed in a tent made of darkroom curtain material. This tent protected the table area from air currents which would interface with the holographic process and also provided a darkroom for development of the photographic plates.

The holograms were made on Agfa-Gevaert Holotest plates, Type 8E75. Plate exposure time was determined from light-meter readings with a typical exposure being about 75-90 s. During exposure, the plates were placed in a plate holder of a design similar to that proposed by Abramson.[1] This plate holder not only holds the plate stable during exposure, but allows accurate repositioning of the plates both for reconstructing the holographic image and for assembling the sandwich hologram.

The exposed plates were developed to 50-percent density, measured by eye, in Kodak D-19 developer. In place of a fixer, a desensitizing solution made of phenosafranine ($C_{18}H_{15}ClN_4$), methanol, and water[6] was used to prevent shrinkage of the emulsion which might introduce errors. After development and desensitizing, the plates were washed for 15 minutes, squeegeed and allowed to dry.

Making and Assembling the Sandwich Holograms

Sandwich holograms are made from two plates, a front plate and a back plate. Each plate is a hologram recording the object in a different state of deformation. Front plates and back plates are made differently[1] and cannot be interchanged, i.e., a sandwich must have a front and back plate, two front or two back plates will not work.

Before any holograms were made, the specimen was placed under a 400-pound (1.8-kN) preload. This preload was necessary to keep the specimen optically stable. After the preloading, the tension in the strain-gaged steel bars was adjusted by tightening or loosening the nuts on the end of the bars, until all four bars had approximately the same tension.

The load on the concrete was then increased in approximately 100-pound (0.45-kN) increments and a hologram made after each increment. Front and back plates were made in alternate increments so that a sandwich could be made by combining a plate with the plate made in the

TABLE 2—SPECIMEN SENSITIVITY VECTOR

Date of Test	Ψ* degree	α† degree	Accuracy‡ In-Plane 10^{-5} in.	In-Plane μm	Out of Plane 10^{-5} in.	Out of Plane μm
1-8-87	70	20	2.0	.5	0.7	0.15
1-30-87	63	27	1.6	.4	0.8	0.2
1-31-87	63	27	1.6	.4	0.8	0.2
2-15-87	90	3	0	0	0.6	0.15

Ψ is the angle between the sensitivity vector k and the object surface.

† α is the half angle between illuminating and reflected beams

‡Accuracy given assumes fringe pattern can be read to ½ fringe, where a fringe is defined as one dark and one light band.

preceding and succeeding increment. This procedure was continued until the specimen failed.

The sandwich holograms were assembled by placing the front and back plate in the plate holder to align them, and then gluing the plates together. Because each plate had to be used in more than one sandwich, the plates could not be permanently glued together, so a hot melt glue was used. This glue was a plastic-like substance which had enough tack to hold the plates securely, but was easily removable. After gluing, the sandwich was placed in a tilting device and illuminated by the reference beam. The tilting device could then be used to manipulate the sandwich and eliminate the rigid-body motion.

Reading the Holograms

Figure 4(a) shows an interferogram of the specimen before the rigid-body motion has been removed. This hologram was made with a sensitivity vector at 63 deg to the surface and is therefore sensitive to both in-plane (x direction) and out of plane (z direction) motion. The crack is seen as a discontinuity in the fringe pattern which follows the line of symmetry [also see Fig. 4(b)]. Note that the effect of rigid-body motion is to create a fringe pattern which is closely spaced. This fringe pattern obscures the effects of stress-induced displacements and makes fringe-counting difficult.

Figure 4(b) is the same hologram with the rigid-body displacement removed. With the removal of some of the rigid-body motion, the fringe pattern is now clearer and easier to count. The fringe pattern shows several fringes which end at the crack tip. This indicates that there is a concentration of displacement at or near the crack tip.

Figure 5 shows a hologram of the specimen where the sensitivity vector was 90 deg to the surface, making the hologram sensitive only to the z direction motion. The hologram in Fig. 6 shows ring-like fringes around the crack tip, again indicating displacement concentrated at or near the crack tip. The fringe pattern here is symmetrical, indicating symmetrical z displacements. The symmetrical z displacements, combined with the symmetry of the specimen and the fact that the crack closely follows the line of symmetry (Fig. 6), indicates that an assumption of symmetrical displacements is not unreasonable.

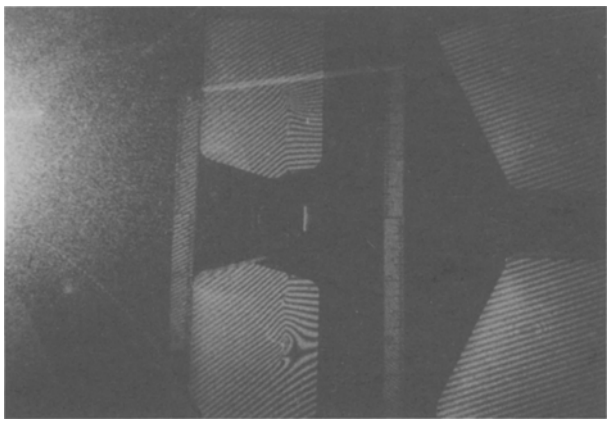

(a)

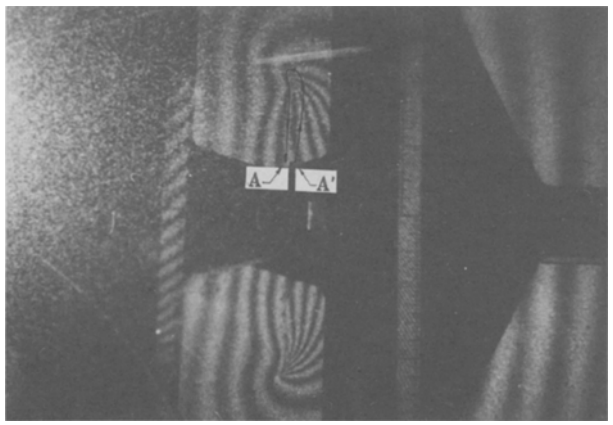

(b)

Fig. 4—Hologram sensitive to X-direction motion, (a) before removal of rigid-body motion, (b) after removal of some rigid-body motion

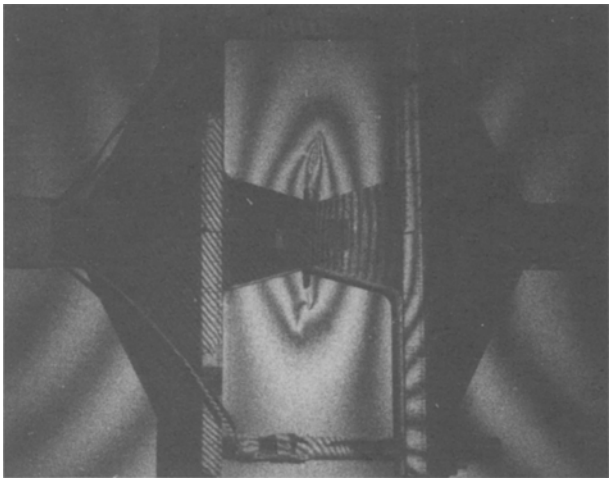

Fig. 5—Hologram sensitive only to Z-direction motion

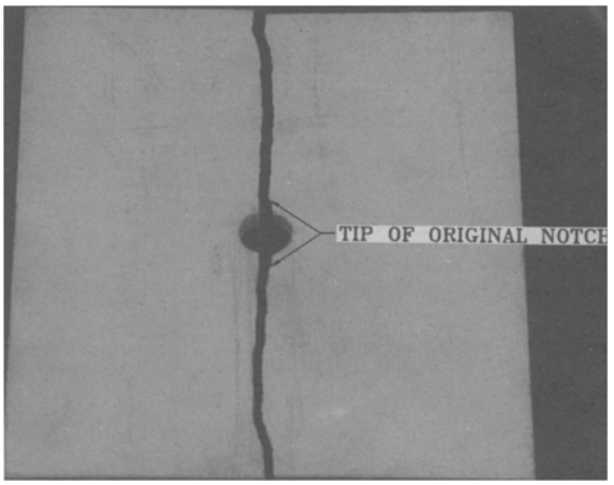

Fig. 6—Failed specimen

Method of Analysis

The fringes in an interferogram represent the projection of the displacement vector on the sensitivity vector. Since there is an infinite number of vectors with the same projection on the sensitivity vector, it is necessary to know the direction of the displacements before eq (2) can be used. However, in certain special cases it is possible to directly separate a desired component of motion without knowing the direction of the displacement beforehand. One such case allows in-plane displacement to be separated directly if the original displacement pattern is symmetric. This method was proposed by Nelson and McCrickerd.[13]

The method described by Nelson and McCrickerd in their paper was not the most general case. The authors have solved the problem for the more general case. Consider two points on the surface of the object, A and A′ [Fig. 4(b)]. From eq (2),

$$\vec{d}_{A'} \cdot \vec{k} = \frac{n_1 \lambda}{2 \cos \alpha} \tag{3a}$$

$$\vec{d}_{A} \cdot \vec{k} = \frac{n_2 \lambda}{2 \cos \alpha} \tag{3b}$$

Subtracting yields

$$(\vec{d}_{A'} - \vec{d}_{A}) \cdot \vec{k} = \frac{\Delta n \lambda}{2 \cos \alpha} \tag{3c}$$

In a specimen with symmetrical displacements where A and A′ are symmetrical points, $\vec{d}_{A'} - \vec{d}_{A}$ is the x direction component of displacement (Fig. 7) and Δn is the number of fringes between points A and A′. The x displacement measured from the line of symmetry is given by

$$x = \frac{\Delta n \lambda}{4 \cos \alpha \cos \Psi} \tag{4}$$

where Ψ = angle between $\vec{k}$ and the x axis.

To understand what this means, it is convenient to think of the fringe pattern as a contour map in which each fringe represents a change in 'elevation'. The information desired is the difference in 'elevation' between two mirror-image points. If, for example, it was desired to know the in-plane displacement between point A′ and A in Fig. 4(b), one would trace a path from point A′ to A, being sure not to cross any edges or discontinuities (cracks), and counting the number of fringes crossed. It is also necessary to keep track of the signs of the fringes (whether one is going 'uphill' or 'downhill'). The sign of the fringes is found by giving the hologram a slight tilt and watching how the fringes move. Fringes with the same sign move in the same direction while fringes with opposite signs move in opposite directions. Also, if any part of the path begins and ends on the same fringe, the net fringe count between those two points must be 0.

In Fig. 4(b), points A and A′ are on a bright fringe, but it is not the same fringe at both points since the crack separates points A and A′. Tracing a path around the crack it is found that there are five fringes between points A′ and A (a fringe is a light and dark band). The displacement between A and A′ is

$$\lambda = 2.5 \times 10^{-5} \text{ in. } (.633\ \mu\text{m})$$

$$\alpha = 27 \text{ deg} \qquad \Psi = 63 \text{ deg}$$

$$d = \frac{5(2.5 \times 10^{-5})}{2 \cos (27) \cos (63)} \times 15.5 \times 10^{-5} \text{ in. } (4\ \mu\text{m})$$

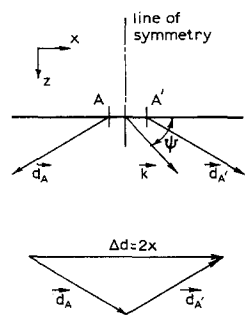

Fig. 7—Subtraction of symmetrical displacement vectors to yield X-direction motion

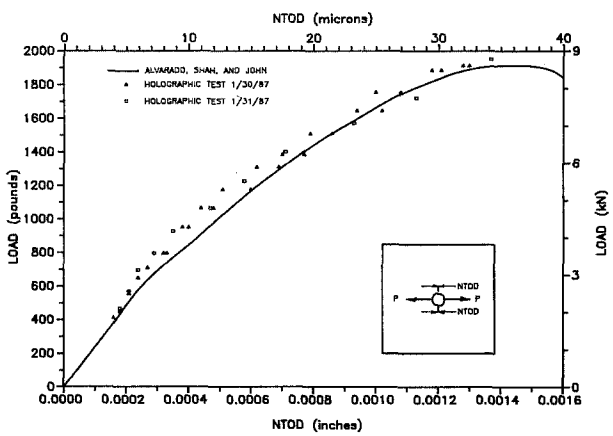

Fig. 8—Load versus notch-tip-opening displacement (NTOD)

Accuracy

The fringe counts and measurement of crack length were accomplished by photographing the holograms. The crack lengths were measured both by scaling off the photograph and by using rulers which had been glued to the airplane-shaped pieced and 'hologrammed' along with the specimen. The crack lengths were measured to the nearest 1/8 in. (3 mm). The fringes were counted to the nearest 1/2 fringe, with a fringe being one light and one dark band. The accuracies can be found from eq (4) and are given in Table 2.

Tilting the holograms to remove rigid-body motion does not affect the fringe count, Δn. The method used gives the vector difference of the motion at two symmetrical points. When measuring crack profiles, the two symmetrical points are so close to each other (they are separated only by the crack width) that both points can be considered to have the same rigid-body-motion vector. When the vector difference is taken the rigid-body motion cancels out. Therefore, the fringe count, Δn, is the same regardless of the tilt of the hologram. This was confirmed by the authors.

Verification of the Method

To verify the method illustrated, the holographic data were compared with data from Alvarado, Shah and John,[4] who tested the same type of specimen in a closed-loop testing machine. Alvarado *et al.* inserted small clip gages into the precast notch to measure the opening of the notch. Figure 8 shows the load versus holographically

measured notch-tip-opening-displacement (NTOD) curves for the two specimens with the 63-deg sensitivity vector, which were made of the same batch of mortar. The solid line is a load versus NTOD curve measured by Alvarado *et al.* for a specimen which failed at approximately the same peak load. There is excellent agreement between the curves. A similar comparison was made for the specimen tested with the 70-deg sensitivity vector.

Crack Profiles

Once the validity of the method had been established, it was possible to plot the crack profiles. Figures 9(a) and 9(b) show two sets of crack profiles from the in-plane sensitive holograms. In this paper, crack profiles referred to as top crack profiles represent the crack which propagates toward the top of the specimen when the specimen is oriented as shown in Fig. 1. Similarly, the cracks referred to as bottom cracks represent cracks which appear to propagate to the bottom of the specimen.

It can also be observed from the crack profiles shown in Figs. 9(a) and 9(b) that the crack-tip-opening displacements will sometimes increase over several load intervals before the crack propagates. Jenq and Shah[9,10] suggested that there was a critical CTOD needed for crack propagation. Based on beam tests for the same type of mortar, Jenq and Shah proposed a value of 3.8×10^{-4} in. (8.5 μm) for the critical CTOD.

Figure 10 shows a plot of CTOD just before crack propagation versus crack length, a. The value of critical CTOD suggested by Jenq and Shah[10] appears to be too high. Figure 11 is a plot of CTOD of the former crack tip just after propagation versus a. In this case, the value proposed by Jenq and Shah appears to be somewhat closer.

Both Figs. 10 and 11 show a large amount of scatter. This scatter is caused by the fact that holographic interferometry shows only the net movement of a point between the two exposures. Since the CTOD is read only at discrete points in time, there is no way to know if a particular crack tip opened wider before propagation. However, if an upper bound is taken in Fig. 10, the idea of a critical CTOD seems valid and the value of $CTOD_c$ proposed by Jenq and Shah appears correct to an order of magnitude.

Comparison with LEFM

As was previously noted, Alvarado, Shah and John[4] tested similar specimens in a closed-loop testing machine.

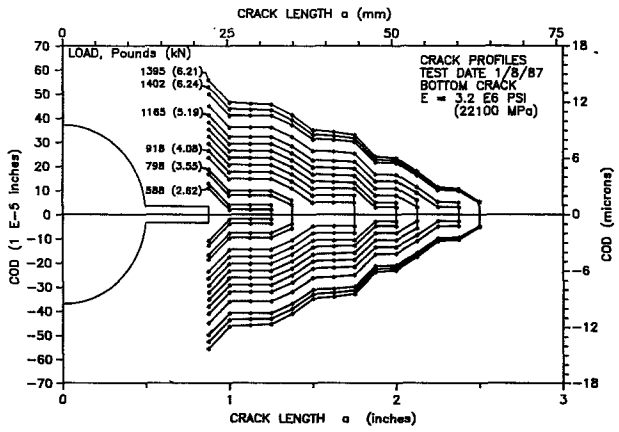

(a)

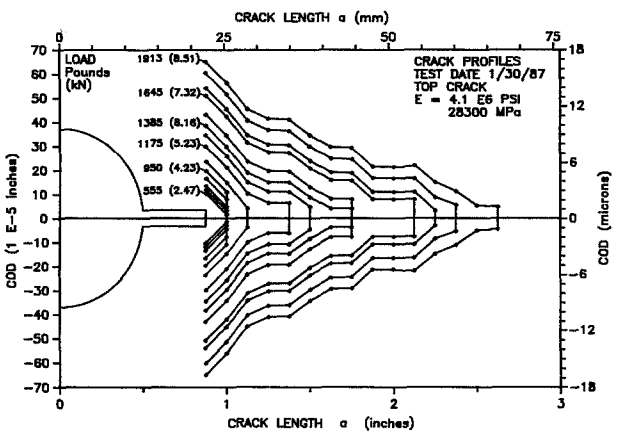

(b)

Fig. 9—Crack profiles

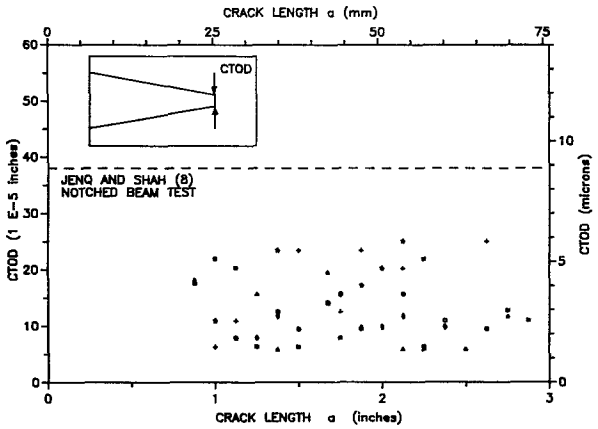

Fig. 10—Crack-tip-opening displacement (CTOD) just before crack propagation versus crack length

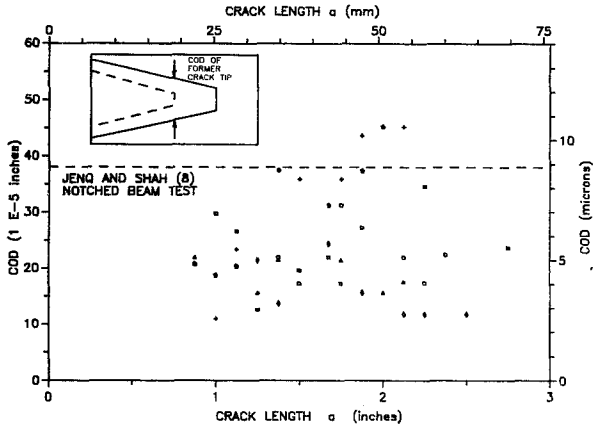

Fig. 11—Crack-opening-displacement (COD) at the former crack tip just after propagation versus crack length

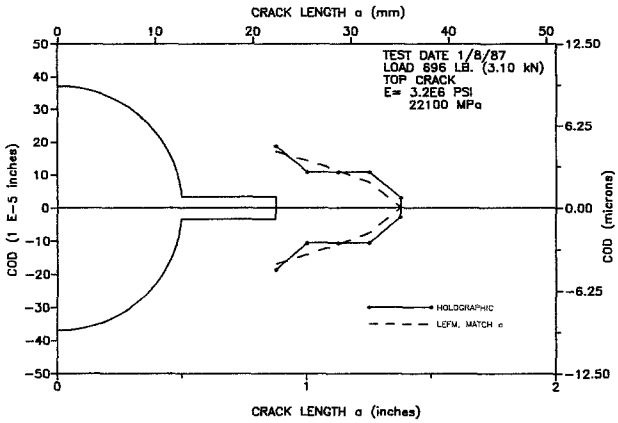

Fig. 12—Comparison of a measured crack profile and the predicted linear-elastic-fracture-mechanics (LEFM) crack profile for a short crack

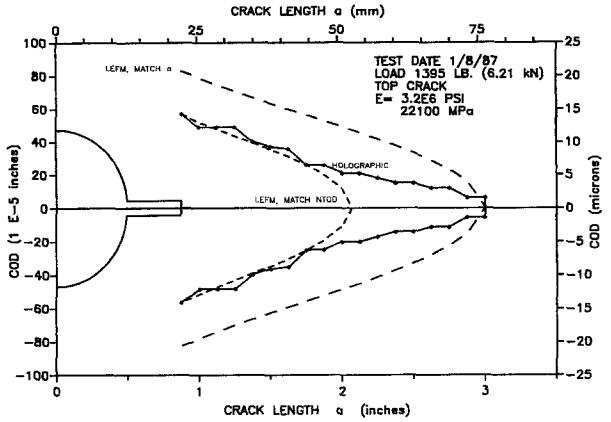

Fig. 13—Comparison of a measured crack profile and the predicted linear-elastic-fracture-mechanics (LEFM) crack profiles for a long crack

During the tests they unloaded the specimen at various points to obtain the effective compliance. Using the compliances obtained from the test Alvarado *et al.* also did a finite-element study of this specimen and obtained expressions for the elastic crack profiles as a function of load and crack length.

Figures 12 and 13 show typical comparisons of measured crack profiles and the LEFM crack profiles obtained by Alvarado *et al.*[4] In Fig. 12, at a load of 696 lb (3.1 kN) (approximately 50-percent peak load for this specimen) there is very little difference between the crack profiles. The difference becomes greater with increasing load and crack length. In Fig. 13, an LEFM crack of the correct length is too wide, while a crack with the correct NTOD is too short. It appears that LEFM cracks with the same crack length must be squeezed in order to match holographic measurements as the crack lengths become longer. This may indicate an increasing influence of a fracture process zone with increasing load, which appears as a closing pressure on the crack as suggested by Hillerborg *et al.*[7]

Conclusions

(1) Holographic interferometry can be used to measure crack profiles in mortar to an accuracy of 1.4×10^{-5} in. (.4 μm). (2) Displacement of cracks in mortar appears to be concentrated at the crack tip. (3) There seems to be a limit as to how large the crack-tip-opening displacement can become before propagation of the crack. Although the data presented here show considerable scatter, the value of critical crack-tip-opening displacement suggested by Jenq and Shah[10] of 3.8×10^{-4} in. (8.5 μm) appears correct to an order of magnitude. (4) At low load levels and corresponding short crack lengths, there is little difference between measured crack profiles and profiles predicted by LEFM. The difference becomes greater under increasing load suggesting that the influence of a fracture process zone becomes greater with increasing load. (5) The holographically measured crack profiles are narrower than predicted LEFM crack profiles with the same crack length. This suggests the presence of a closing pressure on the crack.

Acknowledgment

This research was supported by a grant from the Air force Office of Scientific Research (AFOSR-85-0261) under a program managed by Dr. Spencer T. Wu. The authors are grateful for this support.

References

1. *Abramson, N., The Making and Evaluating of Holograms, Academic Press (1981).*

2. *Abramson, N. and Bjelkhagen, H., "Sandwich Hologram Interferometry. (Part) 5. Measurement of In-plane Displacement and Compensation for Rigid Body Motion," Appl. Opt.,* **18** *(16), 2870 (1979).*

3. *Building Code Requirements for Reinforced Concrete (ACI 318-83), Amer. Concrete Inst., Detroit (1983).*

4. *Alvarado, M., Shah, S.P. and John, R., "Mode I Fracture in Concrete Using Center Cracked Plate Specimens," accepted for publication in J. Eng. Mech. Div., ASCE (March 1988).*

5. *Bazant, Z.P. and Oh, B.H., "Crack Band Theory for Fracture of Concrete," Mat. and Struct.,* **16** *(93), 155-77 (May-June 1983).*

6. *Bjelkhagen, H., "Investigation on the Resolution That Can Be Obtained With the Baltay Holographic Arrangement for the 15-Foot Bubble Chamber," Proc. Phototronics Applied to Nuclear Physics: 2. Nucleophot, CERN-Rep. 85-10:7 (July 1985).*

7. *Hillerborg, A., Modeer, M. and Petersson, P.E., "Analysis of Crack Formation and Crack Growth in Concrete by Means of Fracture Mechanics and Finite Elements," Cement and Concrete Res.,* **6** *(6), 773-782 (Nov. 1976).*

8. *Jaquot, P. and Rastogi, P.K., "Speckle Metrology and Holographic Interferometry Applied to the Study of Cracks in Concrete," Fracture Mechanics in Concrete, ed. F.H. Wittmann, Elsevier Publishers B.V., Amsterdam (1983).*

9. *Jenq, Y.S. and Shah, S.P., "A Fracture Toughness Criterion for Concrete," Eng. Fract. Mech.,* **21** *(5), 1055-1069 (1985).*

10. *Jenq, Y.S. and Shah, S.P., "Two Parameter Fracture Model for Concrete," J. Eng. Mech., ASCE,* **111** *(10), 1227-1241 (Oct. 1985).*

11. *Kesler, C.E., Naus, D.J. and Lott, J.L., "Fracture Mechanics - Its Applicability to Concrete," Proc. 1971 Int. Conf. on Behavior of Mat.,* **IV**, *Japan, 113-124 (1972).*

12. *Kobayashi, A.S., Hawkins, N.M., Barker, D.B. and Liaw, B.M., "Fracture Process Zone of Concrete," Proc. of NATO Advanced Workshop on Application of Fracture Mechanics to Cementitious Composites, ed. S.P. Shah, NATO-ARW, Northwestern Univ. (1984).*

13. *Nelson, D.V. and McCrickerd, J.T., "Residual-Stress Determination Through Combined Use of Holographic Interferometry and Blind-Hole Drilling,"* EXPERIMENTAL MECHANICS, **26** *(4), 379-385 (Dec. 1986).*

14. *Saouma, V.D., Ingraffea, A.R. and Catalano, D.M., "Fracture Toughness of Concrete: K_{IC} Revisited," J. Eng. Mech. Div., ASCE,* **108** *(EM6), 1152-1166 (1982).*

15. *Wecharatana, M. and Shah, S.P., "Prediction of Non-Linear Fracture Process Zone in Concrete," J. Eng. Mech. Div., ASCE, 1100-1113 (June 1983).*